LETTER

doi:10.1038/nature21687

ENL links histone acetylation to oncogenic gene expression in acute myeloid leukaemia

Liling Wan[1,2,3]*, Hong Wen[4,5]*, Yuanyuan Li[6,7]*, Jie Lyu[8], Yuanxin Xi[8], Takayuki Hoshii[2,3], Julia K. Joseph[1], Xiaolu Wang[4], Yong-Hwee E. Loh[9], Michael A. Erb[10], Amanda L. Souza[10]†, James E. Bradner[10,11]†, Li Shen[9], Wei Li[8], Haitao Li[6,7]§, C. David Allis[1]§, Scott A. Armstrong[2,3]§ & Xiaobing Shi[4,5,12]§

Cancer cells are characterized by aberrant epigenetic landscapes and often exploit chromatin machinery to activate oncogenic gene expression programs[1]. Recognition of modified histones by 'reader' proteins constitutes a key mechanism underlying these processes; therefore, targeting such pathways holds clinical promise, as exemplified by the development of bromodomain and extra-terminal (BET) inhibitors[2,3]. We recently identified the YEATS domain as an acetyl-lysine-binding module[4], but its functional importance in human cancer remains unknown. Here we show that the YEATS domain-containing protein ENL, but not its paralogue AF9, is required for disease maintenance in acute myeloid leukaemia. CRISPR–Cas9-mediated depletion of ENL led to anti-leukaemic effects, including increased terminal myeloid differentiation and suppression of leukaemia growth *in vitro* and *in vivo*. Biochemical and crystal structural studies and chromatin-immunoprecipitation followed by sequencing analyses revealed that ENL binds to acetylated histone H3, and co-localizes with H3K27ac and H3K9ac on the promoters of actively transcribed genes that are essential for leukaemia. Disrupting the interaction between the YEATS domain and histone acetylation via structure-based mutagenesis reduced the recruitment of RNA polymerase II to ENL-target genes, leading to the suppression of oncogenic gene expression programs. Notably, disrupting the functionality of ENL further sensitized leukaemia cells to BET inhibitors. Together, our data identify ENL as a histone acetylation reader that regulates oncogenic transcriptional programs in acute myeloid leukaemia, and suggest that displacement of ENL from chromatin may be a promising epigenetic therapy, alone or in combination with BET inhibitors, for aggressive leukaemia.

The YEATS (Yaf9, ENL, AF9, Taf14, Sas5) domain-containing proteins AF9 and ENL are frequently fused with the mixed lineage leukaemia (MLL) protein as a result of *MLL1* (also known as *KMT2A*) chromosomal translocations. The resultant fusion proteins are oncogenic drivers in acute myeloid leukaemia (AML) and acute lymphoid leukaemia (ALL)[5]. To assess the functional importance of the wild-type alleles of *AF9* (*MLLT3*) and *ENL* (*MLLT1*) in *MLL*-rearranged leukaemias, we used a CRISPR–Cas9-mediated gene-editing and negative-selection strategy (Fig. 1a). Cells expressing *ENL* single-guide RNAs (sgRNAs) were outcompeted by non-transduced cells in various *MLL*-rearranged leukaemia cells, whereas sgRNAs targeting *AF9* had little effect on cell growth (Fig. 1a and Extended Data Fig. 1a–d). Using a clonal MOLM-13 cell line in which Cas9 expression can be induced by doxycycline (Dox) administration (iCas9-MOLM-13), we observed a consistent effect of *ENL* sgRNAs on cell growth after Dox treatment (Extended Data Fig. 1e–g). CRISPR–Cas9- or short hairpin RNA (shRNA)-mediated depletion of ENL also impaired the clonogenic potential of MOLM-13 (Fig. 1b) and MV4;11 (Extended Data Fig. 1h, i) cells grown in cytokine-supplemented methylcellulose. ENL depletion increased the surface expression of the myeloid differentiation marker CD11b (also known as ITGAM) (Fig. 1c) and induced a morphological change to a macrophage-like appearance (Extended Data Fig. 1j). Notably, *ENL* sgRNA-induced growth inhibition and differentiation were rescued by the presence of a mouse *Enl* (*Mllt1*) cDNA that contains several mismatches to the human *ENL* sgRNA (Fig. 1d and Extended Data Fig. 1k). In addition to *MLL*-rearranged leukaemias, *ENL* depletion suppressed the growth of non *MLL*-rearranged leukaemia cell lines such as U-937 and K562, but not human cervical adenocarcinoma HeLa or osteosarcoma U2OS cells (Extended Data Fig. 1l–o). *ENL* silencing also had minimal effect on the growth, colony-forming ability or differentiation potential of sorted $Lin^{-}Sca\text{-}1^{+}c\text{-}Kit^{+}$ (LSK) cells that are enriched for haematopoietic stem cells (Extended Data Fig. 1p–r).

To examine the relevance of ENL and AF9 to leukaemia progression *in vivo*, MOLM-13 cells were transduced with different sgRNAs and transplanted into immunodeficient recipient mice. The expression of *ENL* sgRNA resulted in a marked delay in leukaemia progression (Fig. 1e and Extended Data Fig. 2a) and prolonged survival of the recipient mice (Fig. 1f). Although the terminal leukaemia in the *ENL* sgRNA group was composed of predominantly sgRNA-positive cells, these leukaemia cells had similar protein levels of ENL to those from the control group (Extended Data Fig. 2b, c), indicating that the mice succumbed to an outgrowth of cells that escaped ENL depletion. Together, these results suggest a critical requirement of ENL, but not AF9, for AML maintenance *in vitro* and *in vivo*.

To identify the transcriptional pathways controlled by ENL, we performed RNA sequencing (RNA-seq) analyses on iCas9-MOLM-13 cells expressing different sgRNAs. Whereas *AF9* sgRNA caused minimal changes in gene expression, *ENL* sgRNA induction led to differential expression of a subset of genes, but not to global transcriptional dysregulation (Fig. 2a and Extended Data Fig. 3a). The transcriptional programs altered by the two *ENL* sgRNAs were highly correlated (Extended Data Fig. 3b). Gene set enrichment analyses (GSEA)

[1]Laboratory of Chromatin Biology & Epigenetics, The Rockefeller University, New York, New York 10065, USA. [2]Cancer Biology and Genetics Program, Memorial Sloan Kettering Cancer Center, New York, New York 10065, USA. [3]Department of Pediatric Oncology, Dana-Farber Cancer Institute, Harvard Medical School, Boston, Massachusetts 02215, USA. [4]Department of Epigenetics and Molecular Carcinogenesis, The University of Texas MD Anderson Cancer Center, Houston, Texas 77030, USA. [5]Center for Cancer Epigenetics, The University of Texas MD Anderson Cancer Center, Houston, Texas 77030, USA. [6]Beijing Advanced Innovation Center for Structural Biology, MOE Key Laboratory of Protein Sciences, Department of Basic Medical Sciences, School of Medicine, Tsinghua University, Beijing 100084, China. [7]Tsinghua-Peking Joint Center for Life Sciences, Tsinghua University, Beijing 100084, China. [8]Dan L. Duncan Cancer Center, Department of Molecular and Cellular Biology, Baylor College of Medicine, Houston, Texas 77030, USA. [9]Fishberg Department of Neuroscience and Friedman Brain Institute, Icahn School of Medicine at Mount Sinai, New York, New York 10029, USA. [10]Department of Medical Oncology, Dana-Farber Cancer Institute, Boston, Massachusetts 0221, USA. [11]Department of Medicine, Harvard Medical School, Boston, Massachusetts 02115, USA. [12]Genes and Development and Epigenetics & Molecular Carcinogenesis Graduate Programs, The University of Texas Graduate School of Biomedical Sciences, Houston, Texas 77030, USA. †Present addresses: Novartis Institutes for BioMedical Research, Cambridge, Massachusetts 02139, USA (A.L.S., J.E.B.).
*These authors contributed equally to this work.
§These authors jointly supervised this work.

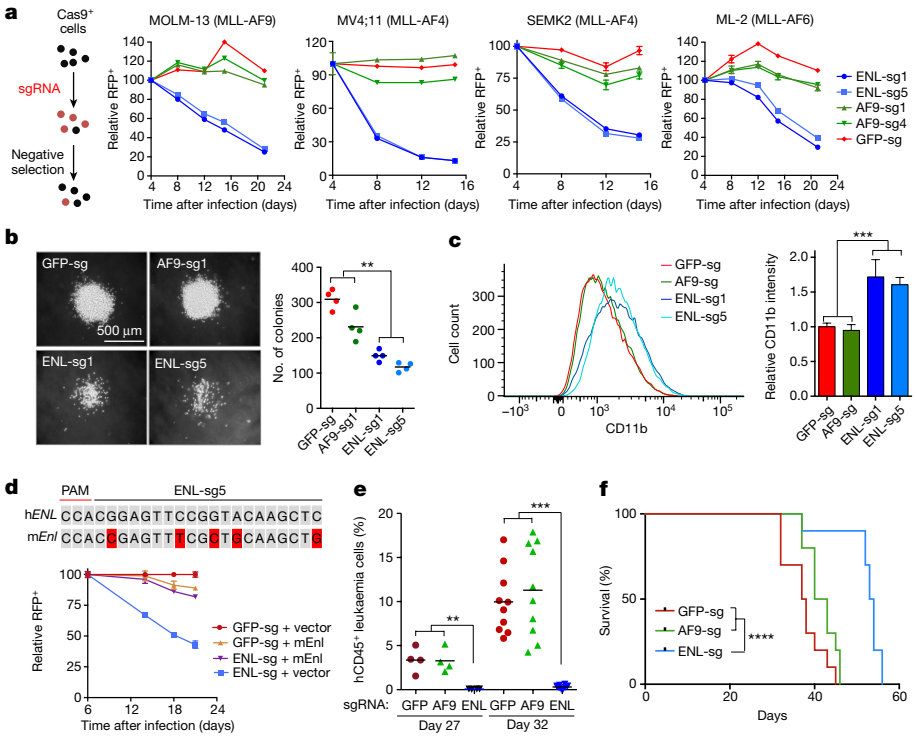

Figure 1 | AML growth is sensitive to ENL depletion *in vitro* and *in vivo*. **a**, Negative-selection competition assay that plots the relative percentage of RFP$^+$sgRNA$^+$ cells over time after transduction of different *MLL*-rearranged leukaemia cell lines with indicated sgRNAs targeting GFP control (GFP-sg), *ENL* (ENL-sg1, ENL-sg5) or *AF9* (AF9-sg1, AF9-sg4). $n = 3$. **b**, Representative images (left) and quantification (right) of colonies formed by MOLM-13 cells transduced with indicated sgRNAs. $n = 4$. **c**, FACS analysis of CD11b surface expression after 4 days of Dox treatment (left) and quantification of CD11b median intensity (right). $n = 4$. **d**, Top, comparison of mouse and human *ENL* sequences at the indicated sgRNA recognition sites. Red nucleotides indicate mismatches. PAM, protospacer-adjacent motif. Bottom, negative-selection competition assay that plots the relative percentage of RFP$^+$sgRNA$^+$ cells after transduction of leukaemia cells with indicated constructs. $n = 3$. **e**, Percentage of human CD45$^+$ cells in the peripheral blood of mice receiving MOLM-13 cells transduced with indicated sgRNAs at day 27 ($n = 4$) or 32 ($n = 10$) after injection. **f**, Kaplan–Meier survival curves of recipient mice ($n = 10$ per group) transplanted with MOLM-13 cells expressing indicated sgRNAs. $P < 0.0001$ using a log-rank test. All error bars represent mean ± s.d. and statistical significance was calculated using two-tailed unpaired Student's *t*-test unless noted otherwise. $^{**}P < 0.01$, $^{***}P < 0.001$, $^{****}P < 0.0001$.

revealed a marked upregulation of the myeloid lineage differentiation signature along with a downregulation of a leukaemia stem cell and MYC-associated gene expression signature[6] in *ENL* sgRNA- or shRNA-expressing MOLM-13 and MV4;11 cells (Fig. 2b and Extended Data Fig. 3c–h), suggesting that ENL is required to sustain the oncogenic gene expression programs crucial for leukaemia maintenance.

ENL resides in large protein complexes termed the super elongation complex (SEC)[7], elongation assisting proteins (EAP)[8] or AF4–ENL–P-TEFb complex (AEP)[9] that contain overlapping subunits such as AFF1–AFF4, ELL, EAF1–EAF2, ENL–AF9 and P-TEFb (for simplicity, we refer to SEC hereafter). To determine the genomic distribution of ENL, we generated stable MOLM-13 and MV4;11 cells ectopically expressing Flag-tagged ENL at levels equivalent to the endogenous ENL proteins, and performed chromatin-immunoprecipitation followed by sequencing (ChIP–seq) experiments. ENL bound to a larger cohort of genes than that of MLL-fusion proteins in both cell lines, suggesting a broader role of ENL than MLL-fusion proteins in transcriptional regulation (Extended Data Fig. 4a, b). There was a greater overlap of ENL-bound genes between the leukaemia cell lines than their overlaps with ENL occupancy in the non-leukaemia HeLa cells (Extended Data Fig. 4c). Notably, the ENL-bound genes in leukaemia cell lines were significantly enriched in pathways implicated in cancer and haematological disease (Extended Data Fig. 4d).

ENL ChIP–seq peaks showed a strong enrichment at promoter regions (transcription start site (TSS) ± 3 kb) (Fig. 2c and Extended Data Fig. 4e), which overlapped with the promoter-proximal RNA polymerase II (Pol II) peak (Fig. 2d and Extended Data Fig. 4f). ENL-bound genes showed a much higher Pol II occupancy than non-ENL-bound genes (Fig. 2e). After ENL depletion, Pol II ChIP–seq signals decreased more prominently on ENL-occupied genes than on non-ENL-bound genes ($P < 0.0001$), including two key AML transcription factors *MYC* and H2.0-like homeobox (*HLX*)[10] (Fig. 2e and Extended Data Fig. 4g, h). The reduction of Pol II occupancy spanned from the promoter proximal region to the 3′ end of gene body, suggesting reduced Pol II activities in both transcriptional initiation and elongation. Indeed, ChIP–seq analyses of the elongation-specific Pol II that is phosphorylated at serine 2 (S2P)[11] showed a markedly decreased occupancy of the elongating Pol II on ENL target genes in ENL-depleted cells (Fig. 2f and Extended Data Fig. 4i). In addition, ENL depletion also resulted in a decrease in the occupancy of CDK9, a SEC component[12] that phosphorylates Pol II at the serine 2 site[13], and the DOT1L-mediated H3K79me2 and H3K79me3 on ENL-target genes (Fig. 2g and Extended Data Fig. 4j, k). Together, these data suggest that ENL regulates gene expression by modulating the recruitment of Pol II through both the SEC and DOT1L complexes.

In light of the AF9 YEATS domain being a reader for histone acetylation[4], we proposed that ENL might link the Pol II transcriptional machinery to chromatin through its YEATS domain. To test this hypothesis, we performed histone peptide array screening and found that the ENL YEATS domain bound specifically to a subset of acetylated histone H3 peptides (Extended Data Fig. 5a). Preferential binding to the H3K27ac, H3K9ac and H3K18ac peptides was further confirmed by peptide pull-down (Fig. 3a) and quantitative isothermal titration calorimetry (ITC) assays (Fig. 3b), with binding dissociation constants (K_d) of 30.5, 32.2 and 50.0 μM for H3K27ac, H3K9ac and H3K18ac, respectively. To explore the underlying molecular basis of this binding specificity, we

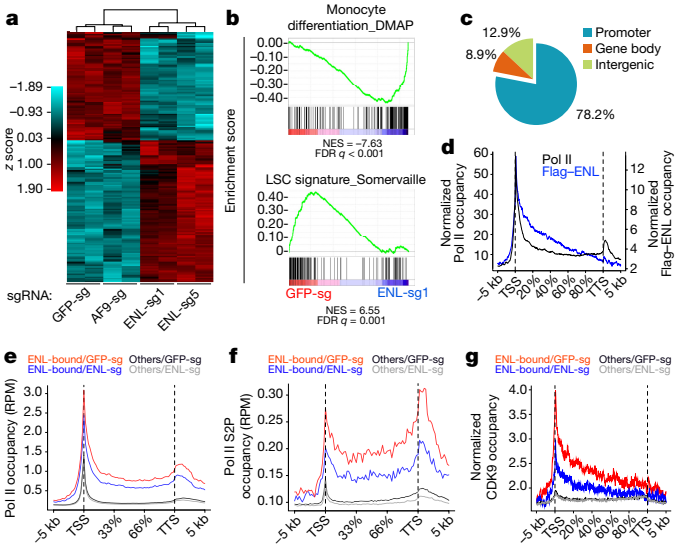

Figure 2 | ENL modulates the recruitment of Pol II to activate oncogenic gene expression. **a**, Heat map representation of genes differentially expressed in iCas9-MOLM-13 cells expressing sgRNAs targeting GFP control, *ENL* or *AF9* (fold change > 1.5 and adjusted $P < 0.05$) 5 days after Dox treatment. Red and green indicate relative high and low expression, respectively. See Supplementary Table 1. **b**, GSEA plots evaluating the changes in monocyte differentiation (top) and leukaemia stem-cell (LSC) gene signatures (bottom) upon ENL depletion. FDR, false discovery rate; NES, normalized enrichment score. **c**, Genomic distribution of Flag–ENL ChIP–seq peaks in MOLM-13 cells. The peaks are enriched in the promoter regions (TSS ± 3 kb). $P < 1 \times 10^{-300}$ (binomial test). See Supplementary Table 3. **d**, Average genome-wide occupancies of Flag–ENL (blue) and Pol II (black) on Flag–ENL-bound genes along the transcription unit. The gene body length is aligned by percentage from the TSS to transcription termination site (TTS). 5 kb upstream of TSS and 5 kb downstream of TTS are also included. **e**–**g**, Average occupancy of Pol II (**e**), Pol II S2P (**f**) or CDK9 (**g**) on Flag–ENL-bound or non-ENL bound genes (others) in iCas9-MOLM-13 cells expressing sgRNAs targeting GFP control or *ENL*. The gene body length is aligned as in **d**. RPM, reads per million.

solved the co-crystal structure of human ENL YEATS bound to the H3K27ac peptide at 2.7 Å (Extended Data Table 1). The ENL YEATS domain adopts an eight-stranded β-sandwich fold (Fig. 3c) with the H3K27ac peptide snugly attached to an acidic surface at the top (Fig. 3d) and the flat acetylamide group of K27ac sandwiched by aromatic residues F59 and Y78 (Fig. 3e). Recognition of the H3K27ac peptide is further stabilized by a network of hydrogen bonds in addition to hydrophobic contacts (Extended Data Fig. 5b). Acetylated histone H3 at K9, K18 and K27 share a common 'R-Kac' recognition signature, in which the '−1' arginine forms a charge-stabilized hydrogen bond with D103 of ENL (Fig. 3e). Structure-based mutagenesis followed by isothermal titration calorimetry (ITC) and peptide pull-down assays revealed a 2.3-fold to more than 17-fold affinity drop or binding elimination upon alanine mutation of the R-Kac-binding residues (Fig. 3f, g).

ChIP–seq analyses of both MOLM-13 and MV4;11 cells revealed that ENL-bound peaks were associated with regions of H3K9ac or H3K27ac modifications (Fig. 3h and Extended Data Fig. 6a). Consistently, the

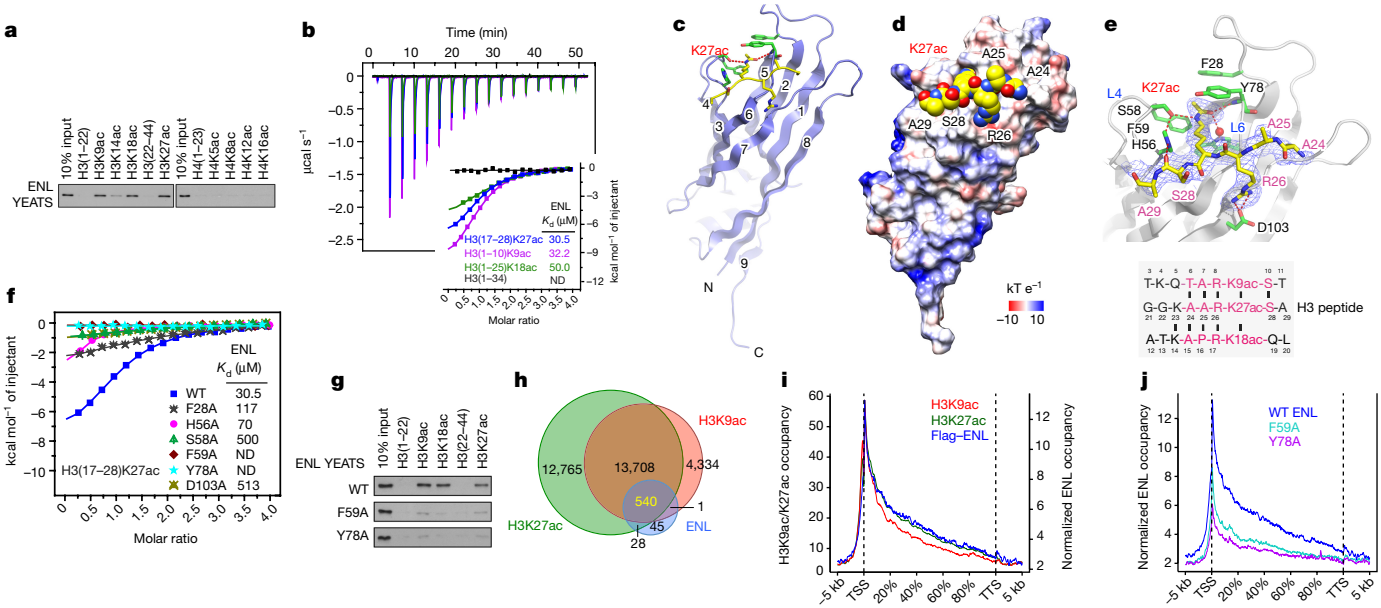

Figure 3 | ENL binds and colocalizes with acetylated histone H3 genome-wide via its YEATS domain. **a**, Peptide pull-down assay of indicated histone peptides and ENL YEATS domain. **b**, ITC titration and fitting curves of human ENL YEATS domain titrated with H3(17–28) K27ac, H3(1–10)K9ac, H3(1–25)K18ac or unmodified H3(1–34) peptides. **c**, Overall structure of the ENL YEATS domain bound to H3K27ac peptide. ENL YEATS is depicted as blue ribbons with key residues highlighted by green sticks. Histone H3K27ac peptide is shown as a yellow ribbon, with side chains highlighted by sticks. Red dashes, hydrogen bonds; red sphere, water molecule. **d**, Electrostatic potential surface of the ENL YEATS domain ranging from −10 to 10 kT e^{-1}. Histone H3 peptide is depicted as space-filling spheres. **e**, Top, hydrogen bonding network between H3K27ac peptide and ENL. Hydrogen bonds are shown as red dashes. Key residues of ENL are depicted as green sticks and labelled black; the H3 peptide is shown as yellow sticks and labelled red. Grey meshes, $F_o - F_c$ omit map countered at 2.0σ level. Bottom, sequence alignment of histone H3 sequences flanking residues K9, K18 and K27. Conserved residues are highlighted in pink. **f**, ITC titration fitting curves of ENL YEATS mutants with H3(17–28)K27ac peptide. **g**, Peptide pull-downs of ENL YEATS mutants and indicated histone H3 peptides. See Supplementary Fig. 1 for gel source data. **h**, Venn diagram showing the overlap of Flag–ENL-, H3K9ac- and H3K27ac ChIP–seq peaks in MOLM-13 cells. $P < 1 \times 10^{-300}$ (three-way Fisher's exact test). See Supplementary Tables 4 and 5. **i**, Average occupancies of Flag–ENL (blue), H3K9ac (red), H3K27ac (green) on ENL-bound genes along the transcription unit. **j**, Average genome-wide occupancies of wild-type (blue) and mutant ENL (F59A in cyan or Y78A in purple) on ENL-bound genes along the transcription unit.

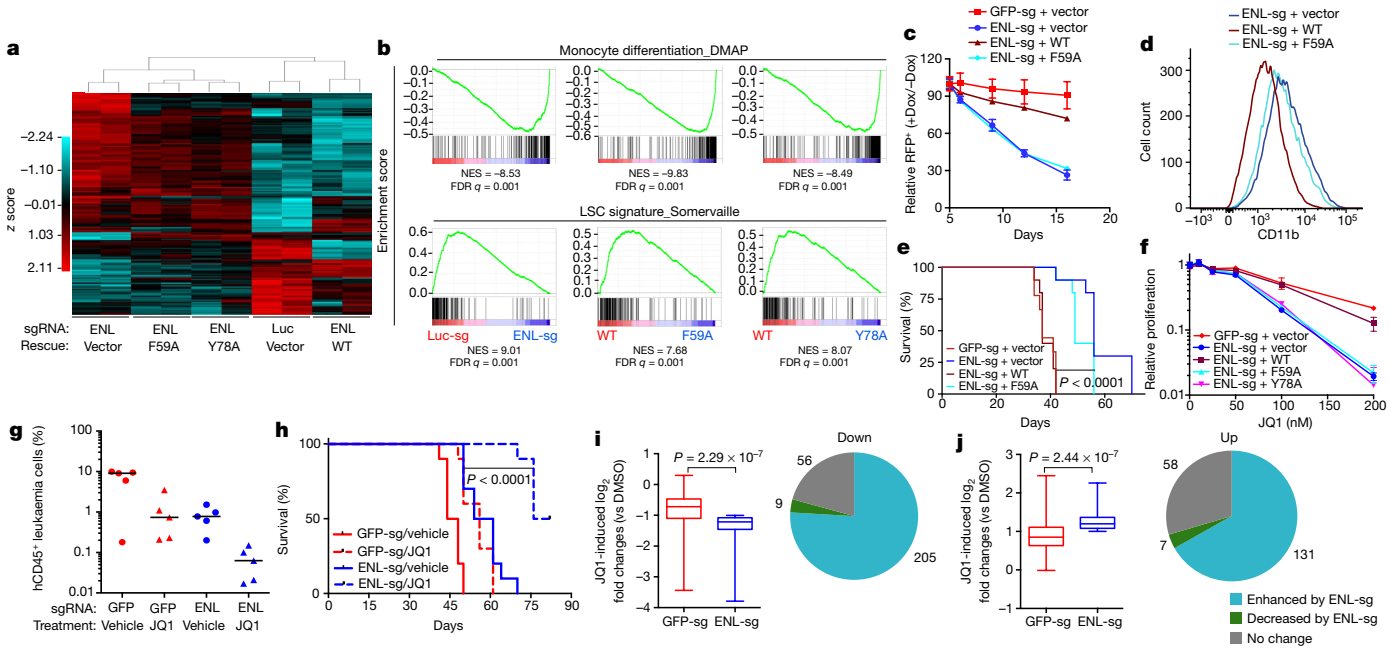

Figure 4 | Disrupting the YEATS-histone acetylation interaction inhibits the functionality of ENL and sensitizes leukaemia cells to BET inhibitors. a, Heat map representation of genes differentially expressed in iCas9-MOLM-13 cells expressing sgRNAs targeting luciferase control or *ENL* (fold change > 1.5 and adjusted $P < 0.05$) in the indicated rescue conditions. **b**, GSEA plots evaluating the changes in monocyte differentiation (top) and leukaemia stem-cell gene signatures (bottom) in the indicated comparisons. **c**, Negative-selection competition assay that plots the relative percentage of RFP^+ $sgRNA^+$ cells after transduction of leukaemia cells with indicated constructs. $n = 3$. **d**, FACS analysis of CD11b surface expression in iCas9-MOLM-13 cells expressing *ENL* sgRNA and indicated mouse *Enl* rescue constructs after 4 days of Dox treatment. See Extended Data Fig. 7b for quantification. $n = 3$. **e**, Kaplan–Meier survival curves of mice ($n = 10$ per group) transplanted with MOLM-13 cells transduced with indicated sgRNAs and rescue constructs. $P < 0.0001$ using a log-rank test. **f**, Effect of JQ1 on the proliferation (normalized to DMSO control) of MOLM-13 cells transduced with indicated sgRNAs and rescue constructs. $n = 5$. **g**, **h**, Leukaemia burden (**g**) and survival curves (**h**) of mice transplanted with iCas9-MOLM-13 cells expressing indicated sgRNAs. Treatment with JQ1 (or vehicle control) and doxycycline was initiated at day 10 after transplantation. **g**, Percentage of human $CD45^+$ cells in the peripheral blood of mice ($n = 5$) at 40 days after transplantation. $P < 0.01$ (*ENL* sgRNA plus JQ1 versus all other groups) using Mann–Whitney test. **h**, Kaplan–Meier survival curves of JQ1-treated mice and vehicle controls ($n = 10$ per group). $P < 0.0001$ (*ENL* sgRNA plus JQ1 versus all other groups) using a log-rank test. **i**, **j**, RNA for RNA-seq experiments was obtained from sorted RFP^+sgRNA^+ iCas9-MOLM-13 cells treated with DMSO or 50 nM JQ1 for 24 h. Genes found to be more than twofold downregulated (**i**) or upregulated (**j**) after JQ1 treatment in *ENL* sgRNA-expressing cells were examined. Left, box plots comparing the JQ1-induced fold changes of these genes in either control (red) or *ENL* sgRNA-expressing (blue) cells. Error bars indicate minimum and maximum, lines denote median, and top and bottom of boxes denote first and third quartile, respectively. $P = 2.29 \times 10^{-7}$ (**i**) and $P = 2.44 \times 10^{-7}$ (**j**) by two-tailed paired Student's *t*-test. Right, pie charts showing the categorization of these genes based on the relationship to ENL depletion. Genes in which the absolute JQ1-induced fold change was more than 1.2-fold higher or lower in *ENL* sgRNA-expressing cells compared to control were classified as enhanced (blue) or decreased (green) by *ENL* sgRNA, respectively. There are significantly more genes in the enhanced than the decreased by *ENL* sgRNA group ($P < 0.0001$ by Fisher's exact test). See Supplementary Table 10. All error bars represent mean ± s.d. ($n = 3$) unless noted otherwise.

average distribution of ENL correlated extremely well with that of H3K9ac and H3K27ac in the region immediately downstream of the TSS (Fig. 3i and Extended Data Fig. 6b, c). Notably, compared to wild-type ENL, the YEATS domain mutants deficient in acetyl-binding exhibited markedly reduced occupancy at ENL-bound genes (Fig. 3j and Extended Data Fig. 6d–f), whereas their interactions with other SEC components were not affected (Extended Data Fig. 6g, h). The ENL YEATS domain is also required for Pol II recruitment, as cells expressing the YEATS mutants exhibited reduced Pol II occupancy on ENL target genes such as *MYC* (Extended Data Fig. 6i). Together, these findings revealed an important 'reader' function of the YEATS domain in mediating the chromatin localization of ENL and the recruitment of the Pol II transcriptional machinery.

To test whether the YEATS domain is required for ENL-dependent maintenance of oncogenic gene expression in leukaemia, we performed rescue experiments with ectopically expressed mouse wild-type or mutant ENL proteins in cells expressing a human *ENL* sgRNA. Transcriptional profiling analyses revealed that wild-type ENL, but not the F59A or Y78A mutant, restored the transcriptional changes caused by the *ENL* sgRNA (Fig. 4a). GSEA analyses further demonstrated the incompetency of these ENL mutants to revert the effect of ENL depletion on the expression of genes involved in crucial cellular processes (Fig. 4b and Extended Data Fig. 7a). Consequently, the mutants were unable to rescue the growth and differentiation defects caused by ENL inhibition (Fig. 4c, d and Extended Data Fig. 7b). In line with these observations, replacement of the ENL YEATS domain with that of AF9 retained the full functionality of ENL (Extended Data Fig. 7c, d). Finally, mice transplanted with *ENL* sgRNA-transduced cells expressing mutant ENL proteins exhibited a marked decrease in leukaemia burden and prolonged survival as compared to the wild-type counterpart (Fig. 4e and Extended Data Fig. 7e). Taken together, these findings demonstrate a crucial role for the ENL YEATS-histone acetylation interaction in regulating oncogenic gene expression and leukaemia maintenance.

Strategies to disrupt the interaction between acetylated histones and their reader proteins, such as the BET family of bromodomain-containing proteins, have been shown to be effective in clinical trials for treatment of a variety of cancers, including haematological malignancies[14]. Interestingly, similar to ENL, BRD4 also associates with P-TEFb and modulates the Pol II transcriptional machinery to regulate key oncogenes such as *MYC*[15]. This finding raised the possibility that ENL and BRD4 might cooperate to sustain optimal oncogenic gene expression programs crucial for leukaemias. In line with this speculation, depletion

of ENL or other SEC components sensitized MOLM-13 cells to the BET bromodomain inhibitor JQ1 (ref. 2; Fig. 4f and Extended Data Fig. 8a). Point mutations disrupting the interaction between the ENL YEATS domain and histone acetylation were sufficient to confer cells with greater sensitivity to JQ1 (Fig. 4f). Increased JQ1 sensitivity by *ENL* silencing was also observed in a panel of leukaemia cell lines, but not in HeLa or U2OS cells (Extended Data Fig. 8b–d). Furthermore, ENL depletion coupled with JQ1 treatment resulted in a significant survival advantage compared with single treatments *in vivo* (Fig. 4g, h and Extended Data Fig. 8e). Mechanistically, ENL depletion markedly enhanced JQ1-induced transcriptional changes in MOLM-13 cells, including *MYC* (Fig. 4i, j and Extended Data Fig. 8f–i), the inhibition of which has been shown to contribute to the sensitivity to BET inhibitors[16,17]. Together, these findings suggest that inhibition of ENL functionality is a potential therapeutic strategy to synergize with BET inhibitors.

Cancer cells often co-opt chromatin regulatory pathways and the general transcriptional machinery to sustain the oncogenic state; hence chromatin and transcriptional regulators are being explored as promising candidate drug targets. Targeting epigenetic readers represents a class of anti-cancer therapy that holds clinical promise. Our study reveals ENL as a chromatin reader that regulates oncogenic programs by linking histone acetylation and the transcription apparatus in AML, thus establishing the ENL YEATS domain as a potential drug target, either alone or in combination with BET inhibitors. Notably, recurrent mutations in the ENL YEATS domain were recently reported in Wilms' tumours[18], suggesting potentially crucial and broad roles of the 'reader' function of ENL in other cancer types that warrant future investigations.

Online Content Methods, along with any additional Extended Data display items and Source Data, are available in the online version of the paper; references unique to these sections appear only in the online paper.

Received 8 May 2016; accepted 3 February 2017.
Published online 1 March 2017.

1. Garraway, L. A. & Lander, E. S. Lessons from the cancer genome. *Cell* **153,** 17–37 (2013).
2. Filippakopoulos, P. *et al.* Selective inhibition of BET bromodomains. *Nature* **468,** 1067–1073 (2010).
3. Dawson, M. A. *et al.* Inhibition of BET recruitment to chromatin as an effective treatment for MLL-fusion leukaemia. *Nature* **478,** 529–533 (2011).
4. Li, Y. *et al.* AF9 YEATS domain links histone acetylation to DOT1L-mediated H3K79 methylation. *Cell* **159,** 558–571 (2014).
5. Deshpande, A. J., Bradner, J. & Armstrong, S. A. Chromatin modifications as therapeutic targets in MLL-rearranged leukemia. *Trends Immunol*. **33,** 563–570 (2012).
6. Somervaille, T. C. P. *et al.* Hierarchical maintenance of MLL myeloid leukemia stem cells employs a transcriptional program shared with embryonic rather than adult stem cells. *Cell Stem Cell* **4,** 129–140 (2009).
7. Lin, C. *et al.* AFF4, a component of the ELL/P-TEFb elongation complex and a shared subunit of MLL chimeras, can link transcription elongation to leukemia. *Mol. Cell* **37,** 429–437 (2010).
8. He, N. *et al.* Human Polymerase-Associated Factor complex (PAFc) connects the Super Elongation Complex (SEC) to RNA polymerase II on chromatin. *Proc. Natl Acad. Sci. USA* **108,** E636–E645 (2011).
9. Yokoyama, A., Lin, M., Naresh, A., Kitabayashi, I. & Cleary, M. L. A higher-order complex containing AF4 and ENL family proteins with P-TEFb facilitates oncogenic and physiologic MLL-dependent transcription. *Cancer Cell* **17,** 198–212 (2010).
10. Kawahara, M. *et al.* H2.0-like homeobox regulates early hematopoiesis and promotes acute myeloid leukemia. *Cancer Cell* **22,** 194–208 (2012).
11. Sims, R. J. III, Belotserkovskaya, R. & Reinberg, D. Elongation by RNA polymerase II: the short and long of it. *Genes Dev.* **18,** 2437–2468 (2004).
12. Luo, Z. *et al.* The super elongation complex family of RNA polymerase II elongation factors: gene target specificity and transcriptional output. *Mol. Cell. Biol.* **32,** 2608–2617 (2012).
13. Peterlin, B. M. & Price, D. H. Controlling the elongation phase of transcription with P-TEFb. *Mol. Cell* **23,** 297–305 (2006).
14. Filippakopoulos, P. & Knapp, S. Targeting bromodomains: epigenetic readers of lysine acetylation. *Nat. Rev. Drug Discov.* **13,** 337–356 (2014).
15. Jang, M. K. *et al.* The bromodomain protein Brd4 is a positive regulatory component of P-TEFb and stimulates RNA polymerase II-dependent transcription. *Mol. Cell* **19,** 523–534 (2005).
16. Rathert, P. *et al.* Transcriptional plasticity promotes primary and acquired resistance to BET inhibition. *Nature* **525,** 543–547 (2015).
17. Fong, C. Y. *et al.* BET inhibitor resistance emerges from leukaemia stem cells. *Nature* **525,** 538–542 (2015).
18. Perlman, E. J. *et al.* MLLT1 YEATS domain mutations in clinically distinctive Favourable Histology Wilms tumours. *Nat. Commun.* **6,** 10013 (2015).

Supplementary Information is available in the online version of the paper.

Acknowledgements We thank H. Li, M. Armstrong, C.-W. Chen, M. Yu, H. Chu, K. Tanaka, D. Peng and T. Scott for discussions and technical supports. We are grateful to The Rockefeller University Genomic Resource Center, Flow Cytometry Resource Center, The MD Anderson Science Park Next-Generation Sequencing Facility (CPRIT RP120348), The Sequencing and Microarray Facility and The Flow Cytometry and Cellular Imaging Core Facility (NIH/NCI P30CA016672), The Shanghai Synchrotron Radiation Facility BL17U beamline, and The China National Center for Protein Sciences Beijing for facility supports. The research was supported by funds from NIH (1R01CA204639-01), the Leukaemia and Lymphoma Society (LLS-SCOR 7006-13), and The Rockefeller University to C.D.A.; NIH grants (CA66996 and CA140575) and the Leukaemia and Lymphoma Society to S.A.A.; grants from NIH/NCI (1R01CA204020-01), Cancer Prevention and Research Institute of Texas (RP160237 and RP170285) and Welch Foundation (G1719) to X.S.; grants from the Major State Basic Research Development Program in China (2016YFA0500700 and 2015CB910503), and the Tsinghua University Initiative Scientific Research Program to H.L.; and grants from NIH (R01HG007538 and R01CA193466) to W.L. X.S. is a recipient of a Leukaemia & Lymphoma Society Career Development Award and an R. Lee Clark Fellow and Faculty Scholar of MD Anderson Cancer Center. L.W. is a fellow of the Jane Coffin Childs Memorial Fund. Y.L. is a Tsinghua Advanced Innovation fellow.

Author Contributions L.W., H.W., Y.L., H.L., C.D.A., S.A.A. and X.S. designed the study, analysed the data and wrote the paper. L.W. and H.W. planned and performed all the molecular, cellular and genomic studies; Y.L. and H.L. performed structural and calorimetric studies; L.W., T.H., M.A.E., A.L.S. and J.E.B. performed mouse xenograft studies; L.W., J.L., Y.X., Y.-H.E.L., L.S. and W.L. performed bioinformatics analysis; J.K.J. and X.W. provided technical assistance; H.L., C.D.A., S.A.A. and X.S. supervised the research.

Author Information Reprints and permissions information is available at www.nature.com/reprints. The authors declare competing financial interests: details are available in the online version of the paper. Readers are welcome to comment on the online version of the paper. Correspondence and requests for materials should be addressed to C.D.A. (alliscd@rockefeller.edu), S.A.A. (scott_armstrong@dfci.harvard.edu) or X.S. (xbshi@mdanderson.org).

Reviewer Information *Nature* thanks R. Agami, J. L. Hess, R. Marmorstein and the other anonymous reviewer(s) for their contribution to the peer review of this work.

METHODS

Plasmids. Mouse wild-type or mutant *Enl* were cloned into pMSCV-IRES-GFP. Human ENL, DOT1L, AFF4, ELL2 and CDK9 cDNA in pENTR or pDONR were purchased from Open Biosystems. The coding sequences in pENTR were subsequently cloned into p3FLAG, pCDH-Flag, or pCAG-Myc destination vectors using Gateway techniques (Invitrogen). Constitutive (pLKO5d.EFS.SpCas9.P2A.BSD, Addgene 57821, a gift from B. Ebert) and inducible (pCW-CAS9, Addgene 50661, a gift from E. Lander and D. Sabatini) Cas9 vectors were used to generate Cas9-expressing cells. All shRNAs targeting human and mouse *ENL* were obtained from Sigma. sgRNAs were cloned into pLKO5.sgRNA.EFS.tRFP657 vector (Addgene 57824, a gift from B. Ebert). All shRNA and sgRNA sequences used are provided in Supplementary Table 11.

Cell culture, virus transduction and functional assays. Human leukaemia cell lines MOLM-13, MV4;11, ML-2, SEMK2, U-937 and K562 were maintained in RPMI 10% FBS supplemented with 2 mM L-glutamine and 100 U ml^{-1} penicillin/streptomycin. HeLa and U2OS cell lines were maintained in DMEM 10% FBS supplemented with 2 mM L-glutamine and 100 U ml^{-1} penicillin/streptomycin. $Lin^{-}Sca\text{-}1^{+}c\text{-}Kit^{+}$ (LSK) cells were freshly sorted from the bone marrow of 6–8-week-old C57BL/6J male mice and cultured in IMDM plus 15% FBS supplemented with 20 ng ml^{-1} mouse SCF (PeproTech), 10 ng ml^{-1} mouse IL-3 (PeproTech) and 10 ng ml^{-1} mouse IL-6 (PeproTech). All cell culture medium contained L-glutamine (2 mM; Gibco), penicillin (100 U ml^{-1}; Gibco), streptomycin (100 μg ml^{-1}; Gibco) and plasmocin (5 μg ml^{-1}; InvivoGen). All human cell lines were mycoplasma-negative and were tested for authentication by short tandem repeat (STR) profiling performed by ATCC or by the MDACC CCSG-funded Characterized Cell Line Core, NCI CA016672.

Lentivirus and retrovirus packaging were performed in HEK293T and Platinum-E cells (Cell Biolabs), respectively, using Lipofectamine 2000 reagent (Invitrogen) in accordance with the manufacturer's instructions. Medium containing virus was concentrated using PEG-it Virus Precipitation Solution (System Biosciences). Spin infection was performed at 1,500 rcf at 35 °C for 90 min and transduced cell populations were usually selected or sorted 48 h after infection.

Competitive proliferation assays using sgRNAs: for constitutive Cas9 expression, cells were analysed for RFP^{+} expression 3 days after infection. For Dox-regulated Cas9 expression cells, cells were analysed for RFP^{+} expression before and after Dox treatment (1 μg ml^{-1}). The percentage of sgRNA-expressing cells (RFP^{+}) was measured over time using flow cytometry and normalized to the starting time point.

Colony-forming assays were performed in Methocult (StemCell Technologies, no. H4435 for human leukaemia cells and M3234 supplemented with 20 ng ml^{-1} mouse SCF, 10 ng ml^{-1} mouse IL-3 and 10 ng ml^{-1} mouse IL-6 for mouse LSKs). Indicated number of cells was resuspended in 100 μl PBS and added to 900 μl Methocult. After 7 days, different types of colony were counted. Cell viability assays for JQ1 treatment were performed using CellTiter-Glo Luminescent Cell Viability Assay (promega/VWR) according to manufacturer's guidelines.

For flow cytometry immunophenotyping, cultured or freshly dissociated cells were collected and stained using the indicated antibodies. Stained samples were analysed on an LSR Fortessa (BD) flow cytometer. Data analysis was performed using FlowJo software.

Antibodies. All antibodies used are provided in Supplementary Table 12.

qRT–PCR analyses. Total RNA was isolated using the RNeasy kit (Qiagen) and reverse transcribed with the high capacity cDNA reverse transcription kit (Applied Biosystems) in accordance with the manufacturer's instructions. Quantitative PCR was performed using the SYBR Green PCR Master Mix (Applied Biosystems) with the StepOne System (Applied Biosystems). qPCR primers used are provided in Supplementary Table 11.

RNA sequencing. RNA was isolated from human leukaemia cells using the RNeasy Mini Kit (Qiagen) and then samples were prepared as instructed using the TruSeq RNA Sample Preparation Kit v2 (Illumina) in accordance with the manufacturer's instructions. RNA-seq samples were sequenced using Illumina NextSeq 500. Raw reads were mapped to human reference genome (hg19) and transcriptome using the TopHat2 package[19]. Transcript abundances were quantified using htseq-count v0.6.0 (ref. 20). Differentially expressed genes were determined using DESeq2 (ref. 21) Genes with a fold change of 1.5 were selected as differential genes. Gene Ontology analysis used the Panther[22] Classification System (http://www.pantherdb.org).

GSEA. GSEA[23] was performed using GSEA v2.2.2 software with 1,000 gene set permutations. Gene sets used were obtained from the Molecular Signatures Database v4.0 (MSigDB, http://www.broadinstitute.org/gsea/msigdb/index.jsp, C2 curated gene sets or C6 oncogenic signatures) or were manually curated from published data set. A detailed description of GSEA methodology and interpretation can be found at http://www.broadinstitute.org/gsea/doc/GSEAUserGuideFrame.html. Normalized RNA-seq data were rank-ordered by expression fold change. Enrichment cores are defined as the members of the gene set that lie before or at the running sum peak (that is, the enrichment score) of the ranked gene list. The normalized enrichment score (NES) provides the degree to which a gene set is overrepresented at the top or bottom of a ranked list of genes. The nominal P value describes the statistical significance of the enrichment score. The FDR q value is the estimated probability that a gene set with a given NES represents a false positive finding. All gene sets used in this study are provided in Supplementary Table 13.

ChIP and ChIP–seq analysis. ChIP analysis was performed essentially as described previously[4]. In brief, cells were cross-linked with 1% formaldehyde for 10 min and stopped with 125 mM glycine. The isolated nuclei were resuspended in nuclei lysis buffer and sonicated using a Bioruptor Sonicator (Diagenode). The samples were immunoprecipitated with 2–4 μg of the appropriate antibodies overnight at 4 °C. Protein A/G beads (Millipore) were added and incubated for 15 min, and the immunoprecipitates were washed twice, each with low-salt, high-salt and LiCl buffer. Eluted DNA was reverse-crosslinked, purified using PCR purification kit (Qiagen), and analysed by quantitative real-time PCR on the ABI 7500-FAST System using the Power SYBR Green PCR Master Mix (Applied Biosystems).

ChIP–seq samples were sequenced using the Illumina Solexa Hiseq 2000 or NextSeq 500. The raw reads were mapped to human reference genome NCBI 36 (hg19) by Solexa data processing pipeline, allowing up to two mismatches. The genome ChIP-seq profiles were generated using MACS 1.3.6 with only unique mapped reads[24]. Clonal reads were automatically removed by MACS. The ChIP–seq profiles were normalized to 20,000,000 total tag numbers, and peaks were called at $P \leq 1 \times 10^{-8}$. Peaks within 1 kb neighbourhood were merged together across multiple samples in the peak overlap analysis.

Peptide microarray and peptide pull-down assay. Peptide microarray and peptide pull-down assays were performed as described previously[25]. In brief, biotinylated histone peptides were printed in triplicate onto a streptavidin-coated slide (PolyAn) using a VersArray Compact Microarrayer (Bio-Rad). After a short blocking with biotin (Sigma), the slides were incubated with the glutathione *S*-transferase (GST)-tagged ENL YEATS domain in binding buffer (50 mM Tris-HCl, pH 7.5, 250 mM NaCl, 0.1% NP-40, 1 mM PMSF, 20% FBS) overnight at 4 °C with gentle agitation. After being washed with the same buffer, the slides were probed with an anti-GST primary antibody and then a fluorescein-conjugated secondary antibody and visualized using a GenePix 4000 scanner (Molecular Devices). For the peptide pull-down assays, 1 μg of biotinylated histone peptides with different modifications were incubated with 1–2 μg of GST-fused proteins in binding buffer (50 mM Tris-HCl, pH 7.5, 300 mM NaCl, 0.1% NP-40, 1 mM PMSF) overnight. Streptavidin beads (Amersham) were added to the mixture, and the mixture was incubated for 1 h with rotation. The beads were then washed three times and analysed using SDS–PAGE and western blotting.

Co-immunoprecipitation. Co-immunoprecipitation was performed essentially as described previously[4]. Cells were lysed in cell lysis buffer containing 50 mM Tris-HCl, pH 7.4, 250 mM NaCl, 0.5% Triton X-100, 10% glycerol, 1 mM DTT, and a complete protease inhibitor tablet (Roche). Antibodies conjugated with protein A/G beads (Millipore) or anti-Flag M2-conjugated agarose beads (Sigma) were incubated with the lysates overnight at 4 °C. The beads were then washed 3–6 times with cell lysis buffer, and the bound proteins were eluted in SDS buffer and analysed by western blotting.

Crystallographic studies. ENL YEATS domain (1–148) and the mutants were recombinantly expressed in *E. coli* and purified as N-terminally His-Sumo-tagged proteins. After Ni column chromatography followed by ulp1 digestion for tag removal, ENL proteins were further purified via ion exchange and size-exclusion chromatography. Before crystallization, ENL sample was mixed with H3(15–39)K27ac peptide in 1:2 molar ratio for about 30 min. Crystallization was performed under 4 °C via vapour diffusion method under the condition: 0.2 M K/Na tartrate, 0.1 M sodium citrate tribasic dihydrate, pH 5.6 and 2 M ammonium sulfate. Diffraction data were collected at Shanghai Synchrotron Radiation Facility BL17U under cryo-conditions. All structures were determined by molecular replacement and refined by the program PHENIX with iterative model building by the program COOT. Detailed data collection and refinement statistics are summarized in Extended Data Table 1.

ITC titration. All ITC titrations were performed under 15 °C using a MicroCal iTC200 instrument. The titration curves were fitted according to the 'one set of sites' binding model. A high-salt titration buffer (500 mM NaCl, 25 mM Tris-HCl, pH 7.5, 2 mM β-mercaptoethanol) was used for ENL YEATS in order to avoid protein aggregation.

Animal experiments. All the mouse experiments were approved by the Institutional Animal Care and Use Committee (IACUC) at Memorial Sloan Kettering Cancer Center and the Dana-Farber Cancer Institute (DFCI). Leukaemia cells (iCas9-MOLM-13) were transplanted by tail-vein injection of 1×10^{6} cells into sub-lethally (2 Gy) irradiated female NSG recipient mice at the age of 6–8

weeks ($n = 10$ per group). Dox-containing chow and water were supplied during the course of the experiments. For JQ1 *ex vivo* treatment trials, leukaemia cells were treated with 1 μg ml^{-1} doxycycline for 2 days and then treated with 100 nM JQ1 and 1 μg ml^{-1} doxycycline for the next 2 days before equal number of viable cells were transplanted. For JQ1 *in vivo* treatment trials, JQ1 was resuspended in DMSO at 200 mg ml^{-1} (for 50 mg kg^{-1} dosing) and then diluted 1:20 with 10.5% (2-hydroxypropyl)-β-cyclodextrin in 0.9% sterile saline. The solution was sonicated until homogenous. Vehicle was prepared and administered the same with the exception that no JQ1 was added. 100 μl doses were administered by intraperitoneal injection for 5 consecutive days with 2-day rest for 30 days starting from day 10 after transplantation. The animals were randomly assigned to the experimental groups. Kaplan–Meier survival curves of mice and the log-rank test were performed using the Prism 6 software program (GraphPad). No animal was excluded from any of the analyses. The investigators were not blinded to allocation during experiments and outcome assessment.

Statistical analyses. Experimental data are presented as mean ± s.e.m. unless stated otherwise. Statistical significance was calculated by two-tailed unpaired *t*-test on two experimental conditions with $P < 0.05$ considered statistically significant unless stated otherwise. Statistical significance levels are denoted as follows: $*P < 0.05$; $**P < 0.01$; $***P < 0.001$; $****P < 0.0001$. No statistical methods were used to predetermine sample size.

Data availability. Structure data has been deposited in Protein Data Bank (PDB) under accession number 5J9S. The ChIP–seq and RNA-seq data have been deposited in the Gene Expression Omnibus (GEO) database under accession numbers GSE80779 and GSE80774, respectively. All other raw data generated or analysed during this study are included in this published article (and its Supplementary Information files).

19. Trapnell, C., Pachter, L. & Salzberg, S. L. TopHat: discovering splice junctions with RNA-Seq. *Bioinformatics* **25,** 1105–1111 (2009).
20. Anders, S., Pyl, P. T. & Huber, W. HTSeq—a Python framework to work with high-throughput sequencing data. *Bioinformatics* **31,** 166–169 (2015).
21. Love, M. I., Huber, W. & Anders, S. Moderated estimation of fold change and dispersion for RNA-seq data with DESeq2. *Genome Biol.* **15,** 550 (2014).
22. Mi, H., Poudel, S., Muruganujan, A., Casagrande, J. T. & Thomas, P. D. PANTHER version 10: expanded protein families and functions, and analysis tools. *Nucleic Acids Res.* **44** (D1), D336–D342 (2016).
23. Subramanian, A. *et al.* Gene set enrichment analysis: a knowledge-based approach for interpreting genome-wide expression profiles. *Proc. Natl Acad. Sci. USA* **102,** 15545–15550 (2005).
24. Zhang, Y. *et al.* Model-based analysis of ChIP-Seq (MACS). *Genome Biol.* **9,** R137 (2008).
25. Wen, H. *et al.* ZMYND11 links histone H3.3K36me3 to transcription elongation and tumour suppression. *Nature* **508,** 263–268 (2014).
26. Bernt, K. M. *et al.* MLL-rearranged leukemia is dependent on aberrant H3K79 methylation by DOT1L. *Cancer Cell* **20,** 66–78 (2011).
27. Guenther, M. G. *et al.* Aberrant chromatin at genes encoding stem cell regulators in human mixed-lineage leukemia. *Genes Dev.* **22,** 3403–3408 (2008).

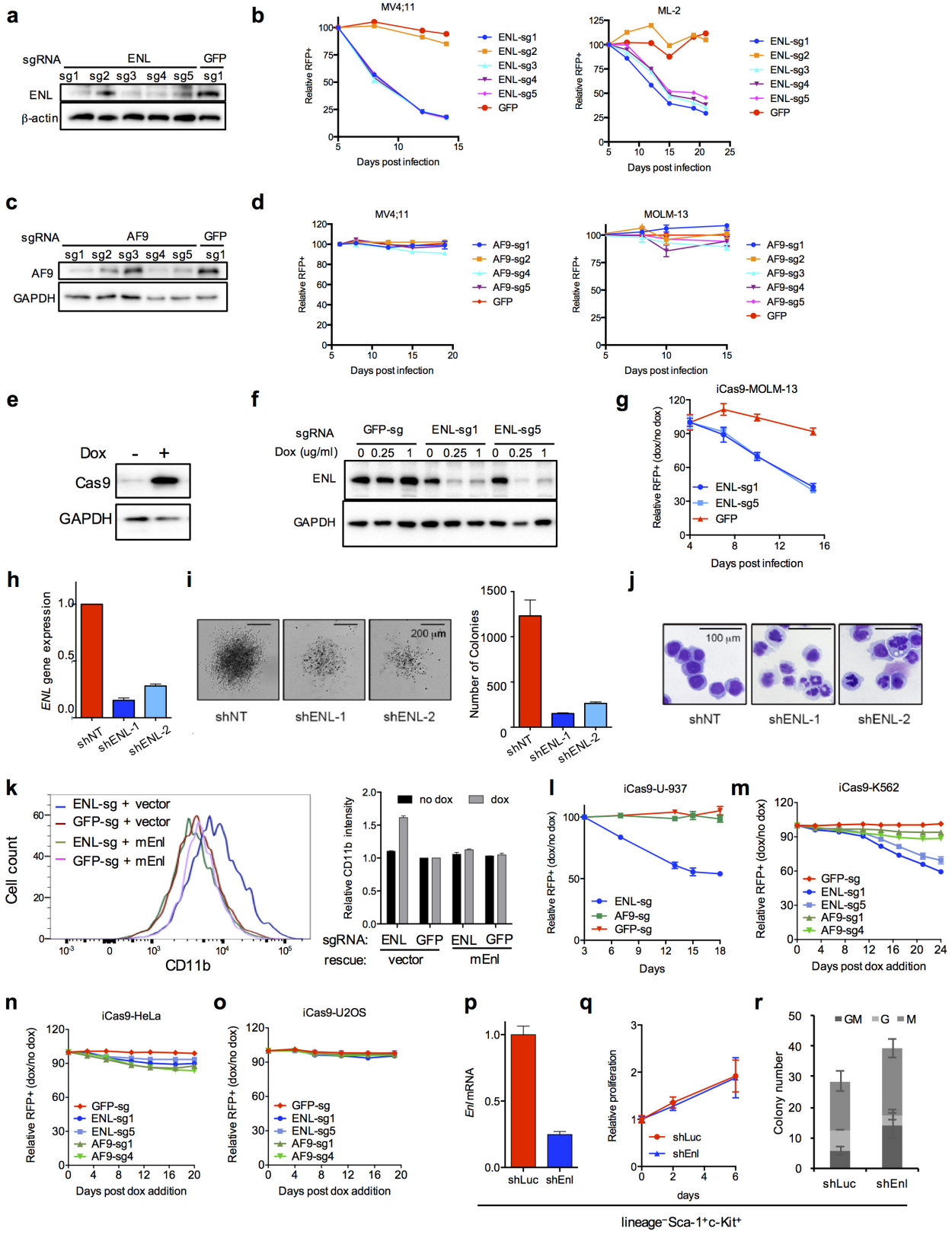

Extended Data Figure 1 | See next page for caption.

Extended Data Figure 1 | Depletion of ENL impairs the growth of AML. a, Western blot demonstrating the knockdown efficiency of five independent sgRNAs (sg1–sg5) targeting *ENL*. **b**, Competition assay that plots the relative percentage of RFP^+sgRNA^+ cells after transduction of leukaemia cells with indicated sgRNAs. $n = 3$. **c**, Western blot demonstrating the knockdown efficiency of five independent sgRNAs targeting *AF9*. **d**, Competition assay that plots the relative percentage of RFP^+sgRNA^+ cells after transduction of leukaemia cells with indicated sgRNAs. $n = 3$. **e**, Western blot demonstrating the induction of Cas9 expression after Dox treatment in iCas9-MOLM-13 cells. **f**, Western blot demonstrating the decrease in ENL protein levels upon Dox treatment in iCas9-MOLM-13 cells. **g**, Competition assay that plots the relative percentage of RFP^+sgRNA^+ cells after Dox treatment in iCas9-MOLM-13 cells. $n = 3$. **h**, Relative *ENL* mRNA levels determined by quantitative PCR after reverse transcription (qRT–PCR) in MV4;11 cells transduced with non-targeting (NT) control or *ENL* shRNAs (shENL-1, shENL-2). **i**, Representative images (left) and quantification (right) of colonies formed by MV4;11 cells transduced with indicated shRNAs. **j**, Light microscopy of May-Grünwald/Giemsa-stained MV4;11 leukaemia cells transduced with control or *ENL* shRNAs. **k**, FACS analysis of CD11b surface expression after 4 days of Dox-induced Cas9 expression (left) and quantification of CD11b median intensity (right) in iCas9-MOLM-13 cells transduced with indicated sgRNAs and rescue constructs. $n = 3$. **l–o**, Negative-selection competition assay that plots the relative percentage of RFP^+sgRNA^+ cells after Dox treatment in iCas9-U-937 (**l**), iCas9-K562 (**m**), iCas9-HeLa (**n**) and iCas9-U2OS (**o**) cells. $n = 3$. **p–r**, LSK cells were sorted from bone marrow of C57BL/6 mice and transduced with luciferase (shLuc) or *Enl* shRNA (shEnl). **p**, Relative *Enl* mRNA levels determined by qRT–PCR quantification after 3 days of drug selection. **q**, Relative proliferation of control (shLuc) or *Enl*-knockout (shEnl) LSKs. $n = 4$. **r**, Quantification of colonies formed by LSK cells cultured for 7 days. $n = 4$. G, granulocyte; GM, colony-forming unit containing granulocyte and macrophage; M, macrophage. All error bars represent mean ± s.d. See Supplementary Fig. 1 for western blot gel source data.

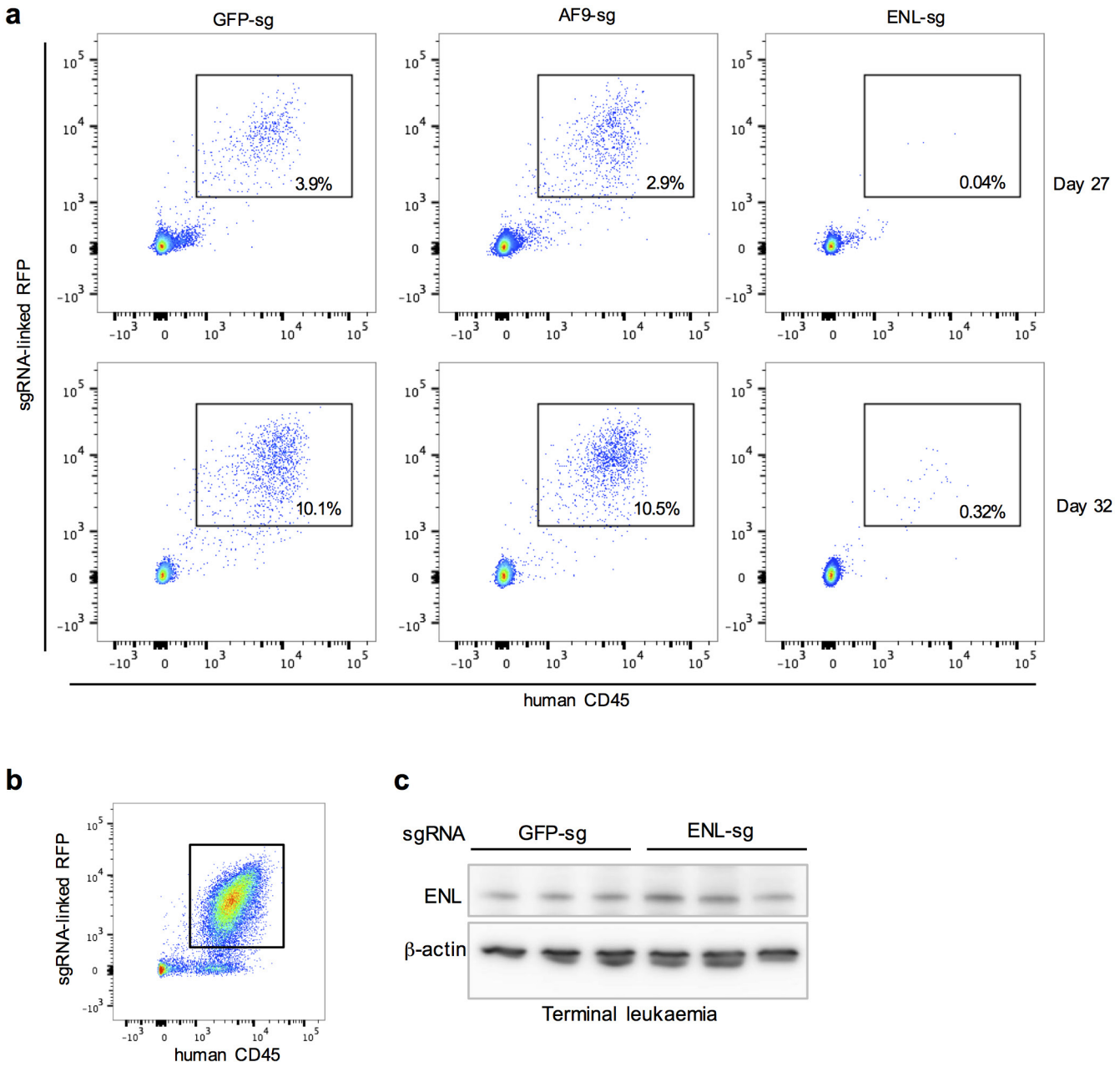

Extended Data Figure 2 | ENL is required for AML growth *in vivo*. **a**, Representative flow cytometry plots of donor-derived (human CD45$^+$) peripheral blood cells 27 or 32 days after transplantation. The gate shown includes RFP$^+$sgRNA$^+$ human leukaemia cells. **b**, Representative flow cytometry plots of bone marrow cells in terminally diseased mice receiving cells transduced with *ENL* sgRNA. Most outgrowing leukaemia cells were RFP$^+$sgRNA$^+$. **c**, Western blot of sorted RFP$^+$sgRNA$^+$ leukaemia cells from terminally diseased mice ($n = 3$) receiving cells transduced with control or *ENL* sgRNA. See Supplementary Fig. 1 for western blot gel source data.

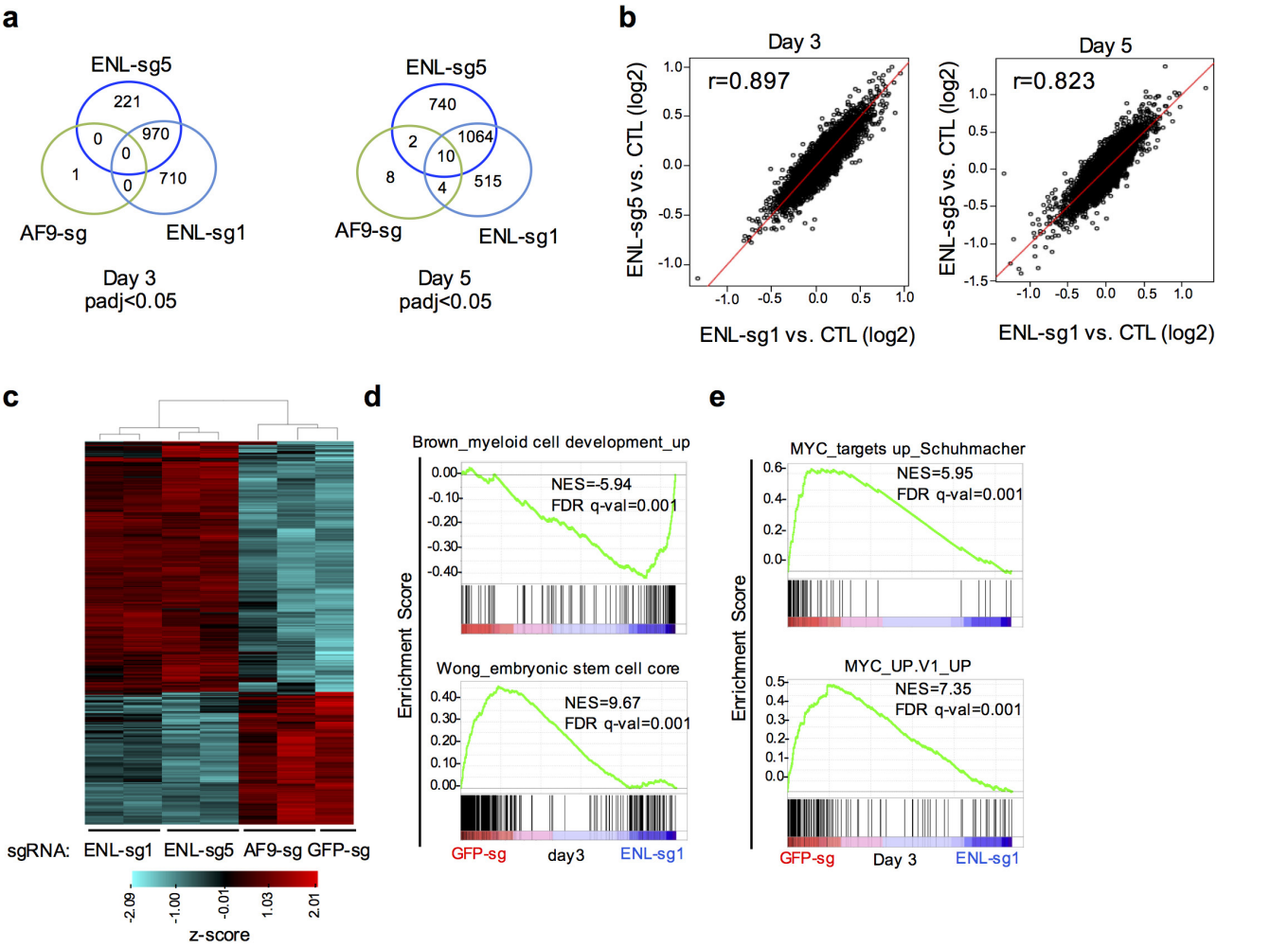

f

ENL-KO-DN genes

GO biological process	Fold enrichment	p-value
DNA-dependent DNA replication	7.35	1.19E-02
double-strand break repair	6.38	4.62E-03
DNA replication	5.11	1.14E-03
regulation of DNA metabolic process	4.76	1.63E-02
nuclear division	4.71	2.62E-04

ENL-KO-UP genes

GO biological process	Fold enrichment	p-value
platelet degranulation	6.71	3.22E-03
integrin-mediated signaling pathway	5.51	2.43E-02
regulation of cell shape	5.1	3.71E-03
exocytosis	4.26	4.37E-05
positive regulation of cell adhesion	3.39	5.09E-04

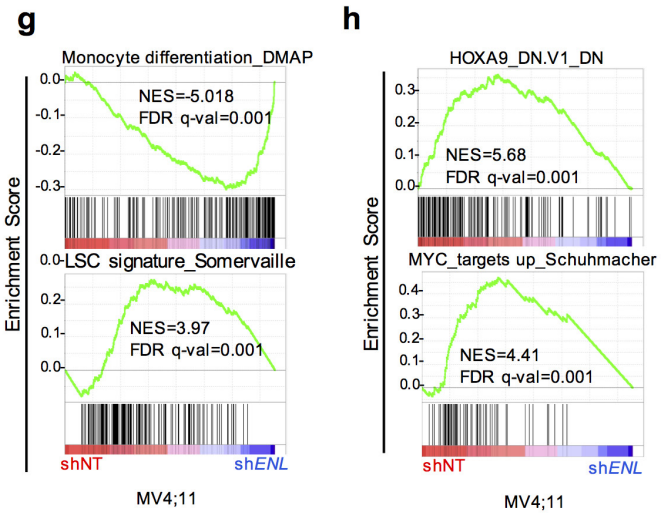

Extended Data Figure 3 | Depletion of ENL deregulates core cellular processes and oncogenic pathways that are required for AML maintenance. a–**f**, RNA for RNA-seq experiments was obtained from sorted RFP$^+$sgRNA$^+$ iCas9-MOLM-13 cells after 3 or 5 days of Dox treatment. **a**, Venn diagram showing the number and overlap of genes for which expression is significantly changed (adjusted $P < 0.05$) upon expression of indicated sgRNAs as compared to GFP control. **b**, Dot plots showing a strong correlation of transcriptional changes ($\log_2$ fold change over GFP control) caused by two independent sgRNAs targeting *ENL*. *r*, correlation coefficient. **c**, Heat map representation of genes differentially expressed between iCas9-MOLM-13 cells expressing sgRNAs targeting GFP control, *ENL* or *AF9* (fold change > 1.5 and adjusted $P < 0.05$) after 3 days of Dox induction. **d**, **e**, GSEA plots evaluating the changes in monocyte differentiation and leukaemia stem cell gene signatures (**d**) and the *MYC* pathways (**e**) upon ENL depletion. **f**, Gene Ontology (GO) term analyses of downregulated (ENL-KO-DN, top) or upregulated (ENL-KO-UP, bottom) genes in *ENL* sgRNA-expressing cells. The top five biological processes that each group of genes were enriched in were shown (details in Supplementary Table 2). Fold enrichment and *P* values are shown. **g**, **h**, RNA for RNA-seq experiments was obtained from MV4;11 transduced with non-targeting (NT) or *ENL* shRNAs. GSEA plots evaluating the changes in monocyte differentiation and leukaemia stem-cell gene signatures (**g**) and the oncogenic pathways (**h**) after *ENL* knockdown.

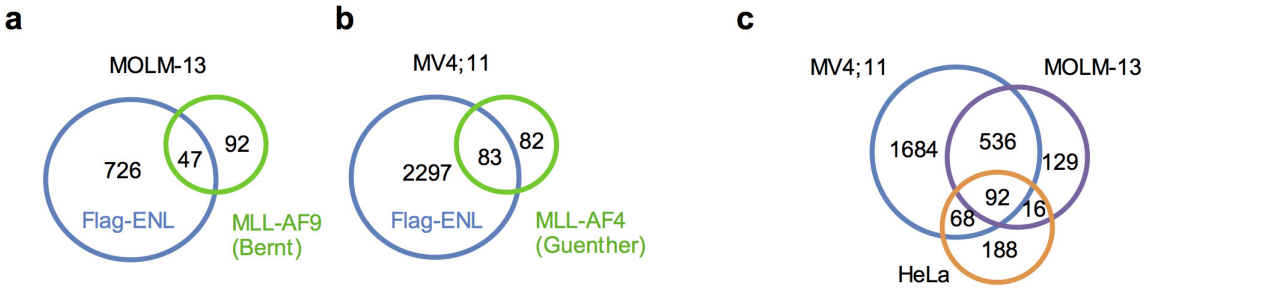

d IPA analysis of the 536 overlapped genes between MOLM13 and MV411 leukaemia cells

Top Diseases and Bio Functions

Diseases and Disorders

Name	p-value	#Molecules
Cancer	8.62E-05 - 1.77E-13	380
Organismal Injury and Abnormalities	8.62E-05 - 1.77E-13	386
Reproductive System Disease	5.49E-05 - 1.77E-13	226
Developmental Disorder	4.34E-05 - 8.13E-12	87
Hematological Disease	8.17E-05 - 7.04E-11	168

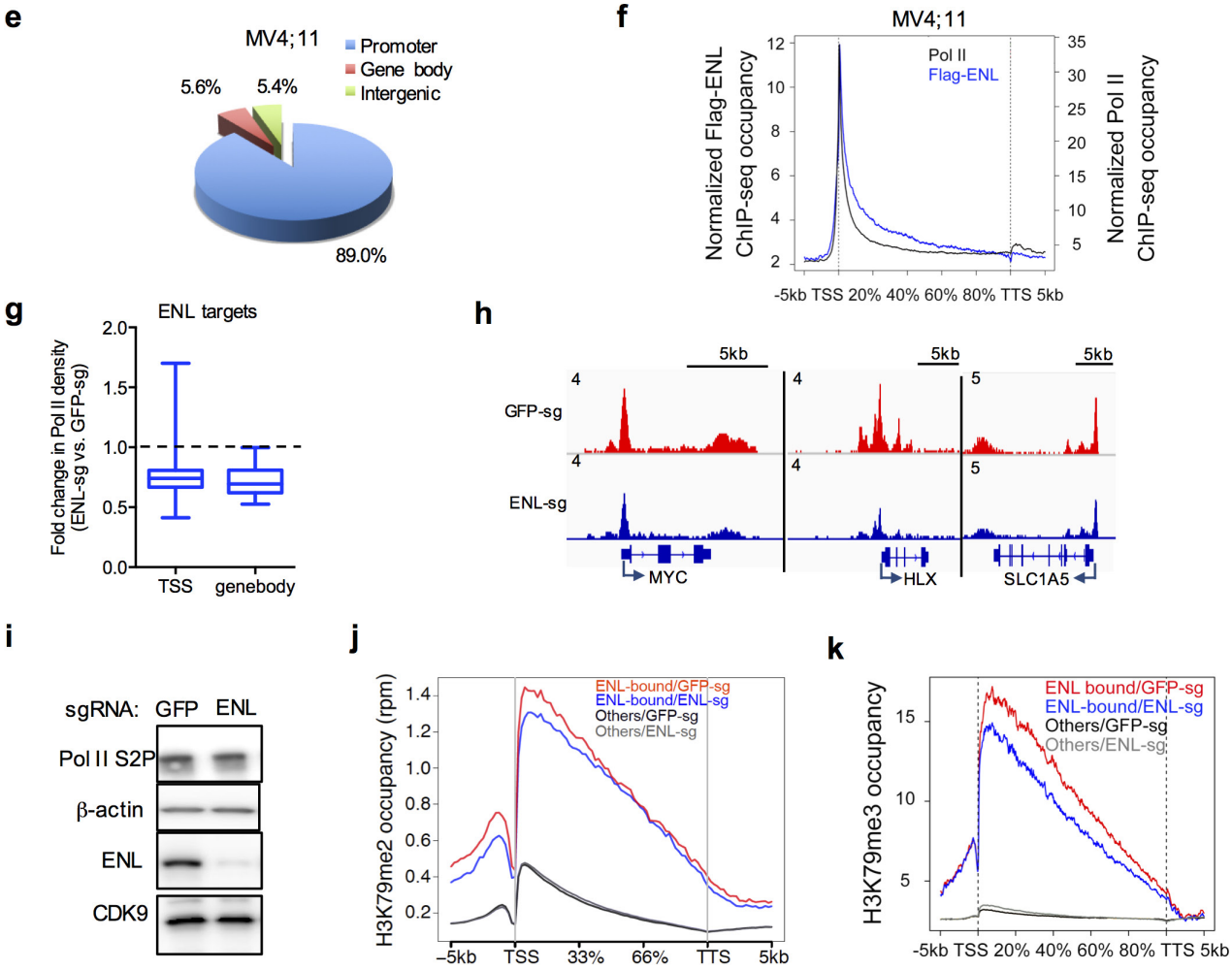

Extended Data Figure 4 | See next page for caption.

Extended Data Figure 4 | ENL depletion decreases the occupancies of total Pol II and Pol II S2P on ENL-bound genes. a, **b**, Venn diagram showing overlaps of Flag–ENL-occupied genes with those of MLL-AF9 in MOLM-13 (ref. 26) (**a**) or MLL-AF4 in MV4;11 cells (ref. 27) (**b**), respectively. **c**, Venn diagram showing overlaps of Flag–ENL-occupied genes in MOLM13, MV4;11 and HeLa cells. See Supplementary Table 7. **d**, IPA analysis of ENL-bound genes overlapped among leukaemia cells but not HeLa cells. **e**, Genomic distribution of Flag–ENL ChIP–seq peaks in MV4;11 cells. The peaks are enriched in the promoter regions (TSS $\pm$ 3 kb). $P < 1 \times 10^{-300}$ (binomial test). See Supplementary Table 6. **f**, Average occupancies of Flag–ENL (blue) and Pol II (black) on Flag–ENL-bound genes in MV4;11 cells along the transcription unit. **g**, Box plots showing the fold changes (normalized to GFP control) of Pol II occupancy at TSS (TSS −30 bp to TSS +300 bp) or the rest of the gene body on ENL-bound and activated genes upon the expression of *ENL* sgRNA. The fold changes at both TSS and gene body were significantly lower than 1 ($P < 0.0001$ by one sample, two-tailed Student's *t*-test). **h**, The genome browser view of Pol II signals in a few of ENL-bound genes (*MYC*, *HLX*, *SLC1A5*) in cells expressing sgRNAs targeting GFP (red) or *ENL* (blue). TSS is indicated by an arrow. **i**, Western blot showing comparable cellular levels of Pol II S2P in MOLM-13 cells expressing sgRNAs targeting GFP or *ENL*. See Supplementary Fig. 1 for gel source data. **j**, **k**, Average H3K79me2 (**j**) and H3K79me3 (**k**) occupancy on Flag–ENL-bound or non-ENL-bound genes (others) in cells expressing sgRNAs targeting GFP control or *ENL*.

a

H3 (1-22)	H3 (1-22)
H3K4me1	H3K4ac
H3K4me2	H3NK9ac
H3K4me3	H3NK14ac
H3K9me1	H3NK18ac
H3K9me2	H3K23ac
H3K9me3	H3K27ac
H3(21-44)	H3 (18-42)
H3K27me1	H3 (21-44)
H3K27me2	H4N(1-23)
H3K27me3	H4NK5ac
H3K36me1	H4NK8ac
H3K36me2	H4NK12ac
H3K36me3	H4NK16ac
H3(67-89)	H2AN(1-22)
H3K79me1	H2ANK5ac
H3K79me2	H2ANK9ac
H3K79me3	H2B(1-22)
H4N(1-22)	H2BK5ac
H4NK20me1	H2BK12ac
H4NK20me2	H2BK15ac
H4NK20me3	H2BK20ac

b

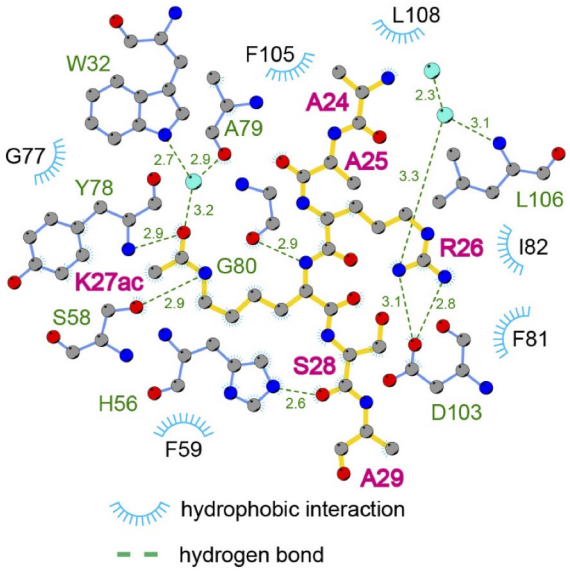

Extended Data Figure 5 | Binding specificity and detail of H3K27ac-bound ENL YEATS complex. a, Histone peptide microarray (detailed annotations on the left) probed with anti-GST antibody against GST–ENL YEATS domain. H3K9ac, H3K18ac and H3K27ac are highlighted in yellow boxes. **b**, LIGPLOT diagrams of H3K27ac-ENL YEATS complex, listing interactions between H3 peptide and ENL YEATS. H3 segments (orange) and key residues of ENL YEATS (blue) are depicted in ball-and-stick mode. Grey ball, carbon; blue ball, nitrogen; red ball, oxygen; large cyan sphere, water molecule. Hydrogen bonds are indicated as green dashed lines with bond length shown in ångströms. Hydrophobic contacts are represented by an arc with spokes radiating towards the ligand atoms they contact, and the contacted atoms are shown with spokes radiating back.

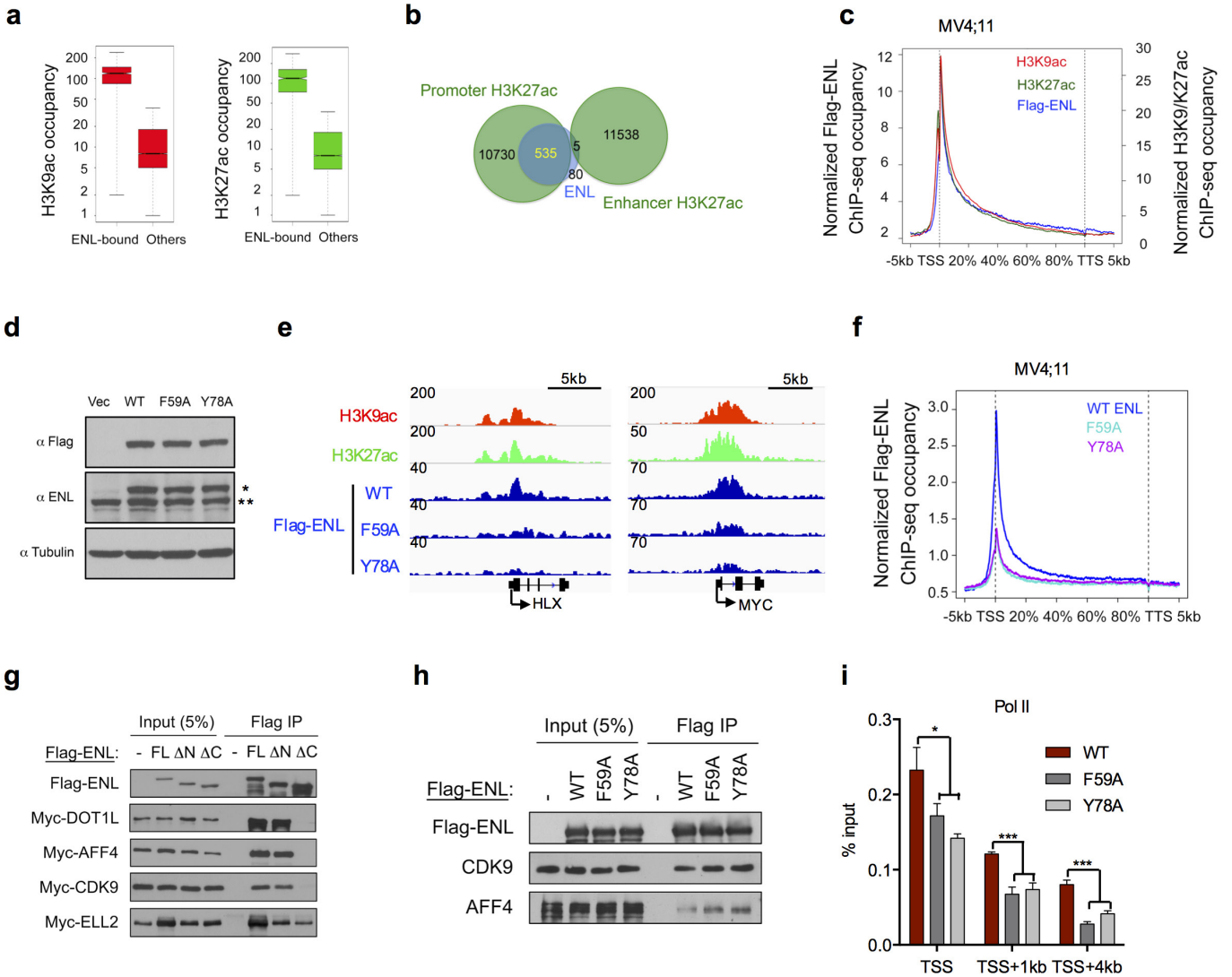

Extended Data Figure 6 | The YEATS domain is required for the chromatin localization of ENL. a, Box plots showing H3K9ac (red) and H3K27ac (green) occupancy in ENL-bound or unbound genes (others) in MOLM-13 cells. $P < 8.1 \times 10^{-152}$ (H3K9ac) and $P < 2.2 \times 10^{-136}$ (H3K27ac) by two-tailed unpaired Student's *t*-test. **b**, Venn diagram showing the overlap of Flag–ENL (blue) and H3K27ac ChIP–seq peaks (green) at promoter or enhancer regions. Promoter H3K27ac is defined as H3K27ac peaks at TSS ± 3 kb regions co-occupied with H3K4me3; enhancer H3K27ac is defined as non-promoter H3K27ac peaks co-occupied with H3K4me1. There is a significant overlap between Flag–ENL and H3K27ac ChIP–seq peaks at TSS ($P = 5.7 \times 10^{-105}$, two-way Fisher exact test) but not at enhancer ($P = 1.0$, two-way Fisher exact test). **c**, Average genome-wide occupancies of Flag–ENL (blue), H3K9ac (red), H3K27ac (green) at Flag–ENL-bound genes along the transcription unit in MV4;11 cells. See Supplementary Tables 8 and 9. **d**, Western blot showing the protein levels of ectopically expressed wild-type or mutant Flag–ENL (marked by asterisk) and endogenous ENL (marked by double asterisk). **e**, The genome browser view of H3K27ac, H3K9ac, Flag–ENL signals in a few of ENL-bound genes (*MYC*, *HLX*). TSS is indicated by an arrow. **f**, Average occupancies of wild-type, F59A or Y78A mutant Flag–ENL on ENL-bound genes along the transcription unit in MV4;11 cells. **g**, Western blot analysis of co-immunoprecipitation using the M2 anti-Flag antibody in cells expressing Flag–ENL and Myc-tagged DOT1L, AFF4, CDK9 or ELL2 proteins. FL, full-length; ΔN, deletion of amino acids 1–113; ΔC, deletion of amino acids 430–559. **h**, Western blot analysis of immunoprecipitation using the M2 anti-Flag antibody in cells expressing wild-type or mutant Flag–ENL. Endogenous CDK9 and AFF4 were assessed. **i**, qPCR analysis of the Pol II ChIP signal in *MYC* gene in *ENL* sgRNA-expressing cells rescued by wild-type or mutant (F59A or Y78A) mouse ENL. Error bars represent mean ± s.e.m. $^{*}P < 0.5$, $^{***}P < 0.001$ (two-tailed unpaired Student's *t*-test). See Supplementary Fig. 1 for gel source data.

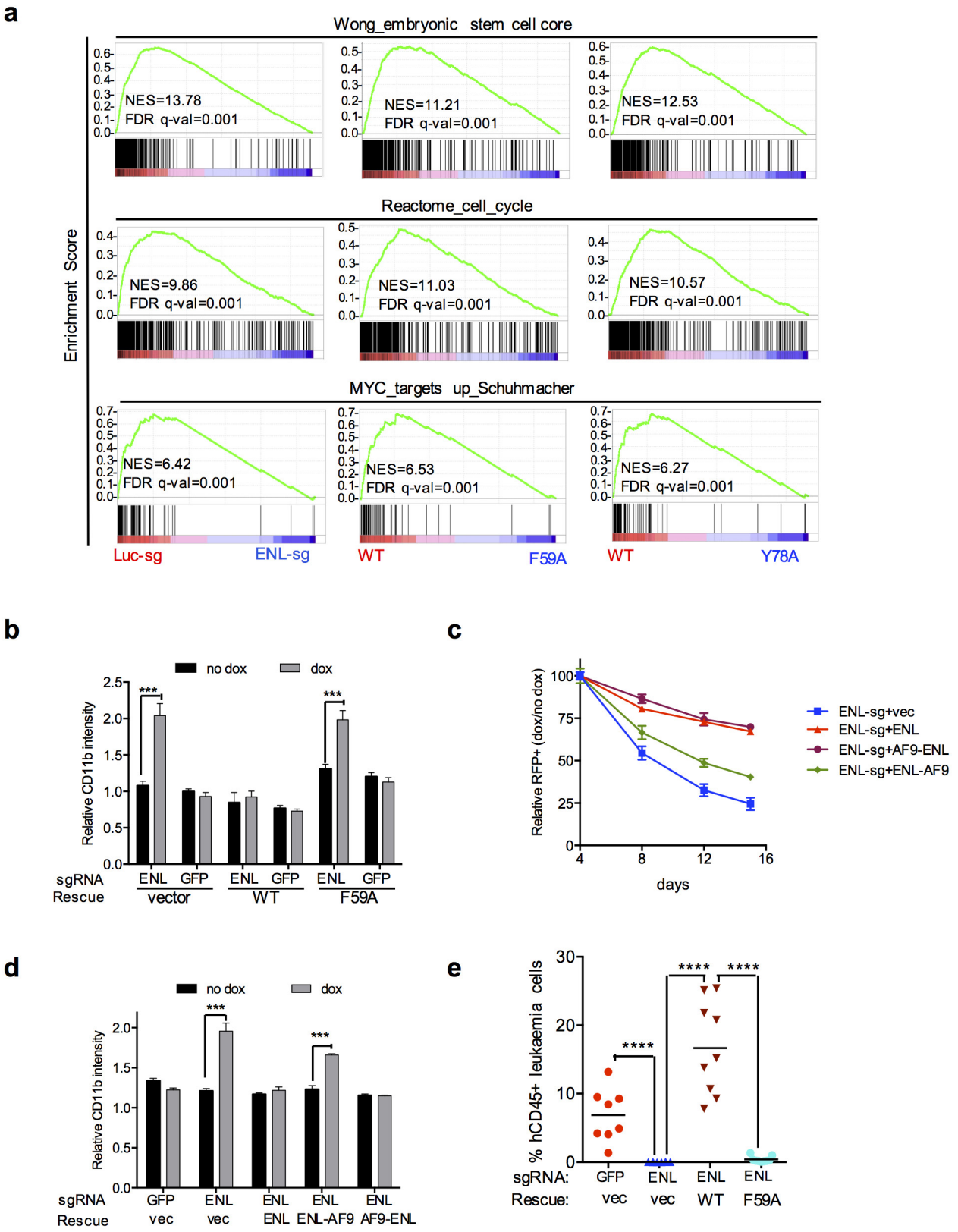

Extended Data Figure 7 | The YEATS domain-histone acetylation interaction is required for the role of ENL in leukaemias. a, GSEA plots evaluating the enrichment of signatures related to stem cells, cell cycle or the *MYC* pathway in the indicated comparisons. **b**, Quantification of CD11b median intensity 4 days after Dox induction in iCas9-MOLM-13 cells transduced with indicated sgRNAs and rescue constructs. $n = 3$. $^{***}P < 0.001$ by two-tailed unpaired Student's *t*-test. **c**, Negative-selection competition assay that plots the relative percentage of $RFP^{+}sgRNA^{+}$ cells after transduction of leukaemia cells with indicated constructs. $n = 3$. **d**, Quantification of CD11b median intensity 6 days after Dox induction in iCas9-MOLM-13 cells transduced with indicated sgRNAs and rescue constructs. $n = 3$. $^{***}P < 0.001$ by two-tailed unpaired Student's *t*-test. **e**, Percentage of human $CD45^{+}$ cells in peripheral blood of mice transplanted with MOLM-13 cells expressing indicated sgRNAs and rescue constructs 30 days after injection ($n \geq 8$). $^{****}P < 0.0001$ by two-tailed unpaired Student's *t*-test. All error bars represent mean ± s.d.

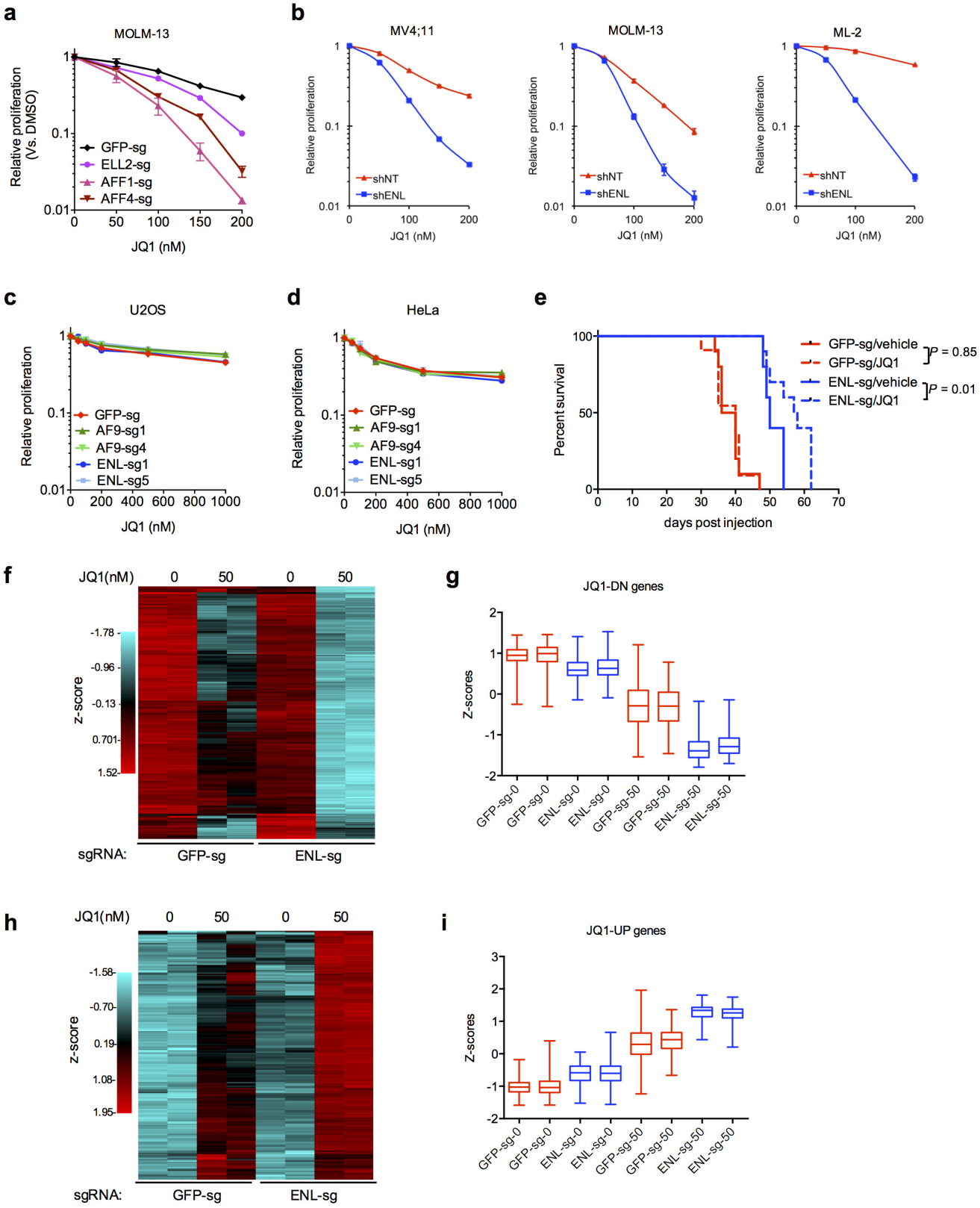

Extended Data Figure 8 | Depletion of ENL increases sensitivity to JQ1 by potentiating JQ1-induced transcriptional changes. a, Effect of JQ1 on the proliferation (normalized to DMSO control) of MOLM-13 cells transduced with indicated sgRNAs targeting SEC components. $n = 5$. **b**, Effect of JQ1 on the proliferation of indicated *MLL*-rearranged leukaemia cells transduced with shNT (red) or shENL (blue) shRNAs. ($n = 3$). **c**, **d**, Effect of JQ1 on the proliferation of indicated non-leukaemia cells (U2OS and HeLa) transduced with *GFP*, *AF9* or *ENL* sgRNAs. $n = 5$. **e**, Kaplan–Meier survival curves of mice ($n = 10$ per group) transplanted with iCas9-MOLM-13 cells expressing indicated sgRNAs and pretreated with doxycycline for 4 days and JQ1 (or DMSO control) for 2 days *ex vivo*. *P* values were calculated using a log-rank test. **f**–**i**, RNA for RNA-seq experiments was obtained from sorted RFP$^+$sgRNA$^+$ iCas9-MOLM-13 cells treated with DMSO (marked as '0') or 50 nM JQ1 for 24 h. Row-normalized heat map (**f** and **h**) and box plots of relative expression levels (*z*-scores, **g** and **i**) of genes found to be twofold downregulated (**f** and **g**) or upregulated (**h** and **i**) after JQ1 treatment in *ENL* sgRNA-expressing cells. All error bars represent mean ± s.e.m.

Extended Data Table 1 | Data collection and refinement statistics

	ENL YEATS-H3K27ac† (PDB code: 5J9S)
Data collection	
Space group	$P3_121$
Cell dimensions	
a, *b*, *c* (Å)	105.0, 105.0, 45.1
α, *β*, *γ* (°)	90, 90, 120
Resolution (Å)	50.00-2.70(2.75-2.70)[a]
R_{sym}	19.5(53.3)
$I/\sigma(I)$	8.5(2.3)
Completeness (%)	98.5(97.7)
Redundancy	4.2(4.0)
Refinement	
Resolution (Å)	40.4-2.7
No. reflections	8,050
R_{work} / R_{free}	18.5/21.6
No. atoms	
Protein	1,249
Peptide/ion(sulfate)	44/20
Water	51
B factors (Å2)	
Protein	22.4
Peptide/ion(sulfate)	34.9/42.4
Water	22.9
R.m.s. deviations	
Bond lengths (Å)	0.003
Bond angles (°)	0.611

* Values in parentheses are for highest-resolution shell.

† One crystal was used for the data collection.

[a] Values in parentheses are for highest-resolution shell.
[b] One crystal was used for the data collection.